

ARE BOTH STARS IN A CLASSIC T TAURI BINARY CLASSIC T TAURI STARS?

L. PRATO¹ AND M. SIMON¹

Astronomy Program, State Univ. of New York, Stony Brook, NY 11794-2100

Received 1996 February 26; accepted 1996 July 17

ABSTRACT

Large near-IR color excesses and emission-line spectra indicate the presence of optically thick circumstellar accretion disks and active boundary layers in young stars. We investigate whether this classic T Tauri (TT) behavior is found in one or both members of a binary system previously identified as a TT on the basis of the unresolved light. We consider the angularly resolved Br γ and, in one case, Na I, spectra of four close (1".3–2".6) TT systems. We also take into account the angularly resolved near-IR ($K-L$) colors of eight additional young binaries with separations between 0".3 and 2".5. We find that for all 12 systems, both components show, or have shown in the history of their observation, evidence for TT behavior. We demonstrate that this cannot be the result of random pairing of a population of single TT and weak-lined T Tauri (WT) stars. We speculate that the result that inner, AU-sized disks tend to survive for a similar length of time in both components of a close (0".3–2".6) binary suggests that a circumbinary envelope effectively regulates the common evolution of the inner disks.

Subject headings: stars: binaries: general — stars: pre-main-sequence

1. INTRODUCTION

In the standard model of star formation, classic emission-line T Tauri stars (TTs) are treated as single, unresolved objects surrounded by accretion disks (Shu et al. 1987). However, recent high-resolution, near-IR (NIR) surveys indicate that a majority of the young stars, at least in the Taurus star-forming region (SFR), are binaries and higher order multiples of typical separation 0".3–0".5 (Ghez, Neugebauer, & Matthews 1993; Leinert et al. 1993; Simon et al. 1995). The circumstellar disks of TTs are believed to contain the material from which planets may form. The evolution of disks in binaries is therefore of considerable interest.

Our understanding of accretion disks and their evolution is improving. Observationally, two regions of circumstellar disks can be distinguished. Inner disks of several AU are characterized by a NIR excess from dust thermal emission in the disk, and a blue excess and emission-line activity from the disk-star boundary layer. Cold dust in outer disks gives rise to millimeter and submillimeter continuum radiation; CO emission is also detected in many outer disks, arising from rotational transitions in cold gas. Outer disks extend from tens to hundreds of AU. Millimeter-wave observations show that outer disks dissipate and evolve more rapidly in binaries than in singles (Osterloh & Beckwith 1994; Jensen, Mathieu, & Fuller 1996; Dutrey et al. 1996), apparently driven by tidal interactions. (In this paper, the term disk will be used to indicate inner disks, unless otherwise noted.) Skrutskie et al. (1990) and Simon & Prato (1995, hereafter SP95) show that, for both singles and binaries, the TT phase as identified for the composite binary system, corresponding to the presence of optically thick disks, varies from 2×10^4 yr to 10^7 yr. The final transition between optically thick and optically thin disks takes place relatively rapidly and is apparently independent of multiplicity (SP95). This paper considers the evolution of individual disks in TT binaries. We already know that in a weak-lined (WT) binary system both objects must be WTs by definition; therefore, if

both stars once had disks and active boundary layers, they are gone in both objects. In a TT system identified as a binary, however, the identity of the individual components is ambiguous. We know that at least one component is a TT, but it is not clear which component, and if the other component is also a TT. Identifying the nature of both components in these systems is necessary in order to begin to understand the pre-main-sequence (PMS) evolutionary process, what drives it, and how multiplicity affects it.

Our approach to the issue of TT phase evolution is to examine the nature of both components in young binary systems, which, unresolved, are characterized as TTs. Because the high angular resolution required to separate the component stars in close binary systems is more readily attainable in the NIR than in the visible, we began by using Br γ emission-line data as a surrogate for H α . The practical difficulties of our initial work limit the present spectroscopic results to four systems, two of which had previously unresolved H α equivalent widths. To enlarge the sample of binaries investigated we adopted the NIR color criterion for TTs described by Edwards, Ray, & Mundt (1993). This enabled us to include an additional eight objects in our analysis. Section 2 describes our approach and observations. In § 3 we present our results. We consider the process of TT evolution and propose a model to account for the evolutionary driving mechanism and briefly consider the implications of our results with respect to possible binary formation mechanisms in § 4. We summarize the results in § 5.

2. DATA

2.1. Approach

We examine systems classified following the convention of the Herbig & Bell (1988, hereafter HBC) catalog which designates PMS stars as TTs and WTs according to whether their H α equivalent width is greater or less than 10 Å. We restrict the sample to binaries of separation less than 3" in order to ensure a very high probability that the two stars form a physical pair. We assume that all TTs evolve into WTs, and that all TTs initially have optically thick accretion disks. In the spectroscopic approach to this study, we

¹ Visiting Astronomer at Infrared Telescope Facility, which is operated by the University of Hawaii under contract to the National Aeronautics and Space Administration.

use the Br γ emission line ($n = 7 \rightarrow 4$) as a NIR surrogate for H α (Table 1). We therefore need an empirical relationship between the Br γ and H α equivalent widths, $W(\text{Br}\gamma)$ and $W(\text{H}\alpha)$ respectively, for TTs. Comparing Br γ data from Greene & Meyer (1995) with H α data from Cohen & Kuhl (1979) and Bouvier & Appenzeller (1991), we estimate an average ratio of $W(\text{H}\alpha)$ to $W(\text{Br}\gamma)$ of ~ 10 . We therefore consider a star a TT if $W(\text{Br}\gamma) \gtrsim 1 \text{ \AA}$. Since the continuum flux in the NIR has a greater excess than that in the region of H α (Strom et al. 1989), we know that $W(\text{Br}\gamma)$ underestimates the importance of the Br γ emission. Therefore, we believe that 1 \AA is a conservative value for the TT cutoff. We obtained calibration spectra of main sequence stars in the range of spectral types of our program objects. The calibration objects are listed in Table 2 and described in § 2.2.

For stars in the Taurus SFR, Edwards et al. (1993) find that $(K-L) > 0.4$ correlates well with $W(\text{H}\alpha) > 10 \text{ \AA}$, and hence is an indicator of classic TT activity. For stellar photospheres in the range of spectral types represented here, we expect $K-L$ values on the order of 0.2 mag. A flat, optically thick reprocessing disk is characterized by $K-L \gtrsim 0.4$, and an optically thin disk by a $K-L$ of 0.2–0.4. Since the Edwards et al. NIR criterion is established only in the Taurus SFR, and may depend on the extent to which the young stars are, on average, obscured in a given SFR, we restrict ourselves to objects located in the Taurus-Auriga

SFR. Relatively few binaries with separations less than 3'' have component resolved K and L band fluxes; we present all of the published data that we obtained in Table 3.

2.2. Observations

We observed the spectroscopic program objects in 1993 May and November at the 3.0 m NASA IRTF using CSHELL, the high spatial and spectral resolution NIR spectrometer (Greene et al. 1993; Tokunaga et al. 1990). We again observed S CrA in 1996 April, and T. Greene provided us with additional observations of VV CrA from 1996 April. At the time of our 1993 observations, CSHELL was equipped with a NICMOS array. The pixel size corresponded to $2.66 \times 10^{-5} \mu\text{m}$ in the direction of the dispersion at the wavelength of Br γ , and 0'.28 along the slit. The seeing was 1''–2'' during the 1993 observations. In systems with separations greater than 1''.5, each component was observed separately using a 1'' slit with a spectral resolution of 20,000. In systems with smaller separations, we aligned the components along the slit and observed both objects simultaneously using a 2'' slit with 10,000 resolution. In 1994, the NICMOS chip was replaced with a 256×256 InSb array, of pixel size $1.52 \times 10^{-5} \mu\text{m}$ in the dispersion direction, and 0'.20 along the slit. We obtained the 1996 observations with this chip, observing each component of S CrA and VV CrA individually with a 1'' slit at 21,500 resolution. Seeing was subarcsecond in 1996 April, and variable around 1'' in 1996 May. We used standard 15'' beam-switching along the slit during all observations. Component separations range from 1'.3 to 2'.6. We observed the Br γ line in all the objects listed in Table 4. In the VV CrA system we also observed the 2.2.07 μm Na I IR doublet in 1993 (see Table 1); each star was observed separately with a 1'' slit at $R = 20,000$. Ar and Kr arc lamp lines, observed each night with a 1'' slit, provided wavelength calibration for both spectral regions. Telluric lines in the target spectra served as a convenient, internal check on the calibrations (Livingston & Wallace 1991).

We observed spectral type standards (Table 2) to provide reference spectra in the Br γ region. Figure 1 shows the spectra of these stars. The heliocentric velocities that we measured agree well with published values. Our high-resolution spectra (20,000) indicate that the photospheric Br γ absorption line is not detectable in dwarf stars of spectral type later than K5. Kleinmann & Hall (1986) demonstrate the same result for dwarf, giant, and supergiants at moderate resolution (~ 3000). Wallace & Livingston (1992) characterize the sunspot spectrum, at resolution $\sim 3 \times 10^5$,

TABLE 1
NIR SPECTRAL LINES OBSERVED

Atom	Transition	λ_{vac} (μm)
H.....	$n = 7 \rightarrow 4$	2.16609
Na I.....	$4p^2P^o_{3/2} \rightarrow 4s^2S_{1/2}$	2.20624
	$4p^2P^o_{1/2} \rightarrow 4s^2S_{1/2}$	2.20897

TABLE 2
Br γ SPECTRAL TYPE STANDARDS

System	Spectral Type	K mag	Reference
SAO 28679.....	G1 Va	5.4	1
BS 4496.....	G8 V	3.5	1
SAO 16306.....	K0.5 V	6.6	1
SAO 28414.....	K2 V	5.9	1
GL 365.....	K5 V	5.5	2

REFERENCES.—(1) Keenan & McNeil 1989; (2) Persson, Aaronson, & Frogel 1977.

TABLE 3
COMPONENT RESOLVED K–L COLORS

System	HBC	Separation (arcsec)	log (age) (yr)	$(K-L)_A$ (mag)	$(K-L)_B$ (mag)	Reference ($K-L$)
(1)	(2)	(3)	(4)	(5)	(6)	(7)
DD Tau.....	30	0.6	5.0	1.7	1.4	2
T Tau.....	35	0.7	5.8	1.0	2.8	4
FV Tau.....	386	0.7	5.8	1.1	1.2	1
Haro 6-10.....	389	1.2	6.3	1.2	3.2	5
DK Tau.....	45	2.5	5.6	1.4	0.9	1
XZ Tau.....	50	0.3	5.3	1.6	0.9	3
CK St 3.....	411	2.0	6.3	1.4	1.3	1
UY Aur.....	76	0.9	5.5	0.7	1.8	2

NOTE.—For T Tau and Haro 6-10, the A component is the optically brighter component.
REFERENCES.—(1) Simon et al. 1995; (2) Tessier, Bouvier, & Lacombe 1994; (3) Haas, Leinert, & Zinnecker 1990; (4) Ghez et al. 1991; (5) Leinert & Haas (1989).

TABLE 4

A. SYSTEM CHARACTERISTICS

System (1)	HBC (2)	Spectral Type (3)	Separation (arcsec) (4)	K_{tot} (mag) (5)	log (age) (yr) (6)	Reference K , age (7)
Haro 6-37.....	73/424	K6/K7	2.6	7.7	5.5	1, 2
AS 205.....	254/632	K0/K5	1.3	5.7	6.0	1, 3
S CrA.....	286	K6	1.4	6.2	4.7	3, 4
VV CrA.....	291	K	1.9	5.9	5.3	3, 4

NOTE.—Spectral types from HBC except for AS 205 (Cohen & Kuhl 1979) and VV CrA (Graham 1992). VV CrA is assumed to be a K4 in order to estimate its age.

B. COMPONENT RESOLVED SPECTROSCOPY

SYSTEM (1)	V_{helio} (km s^{-1}) (2)	$W(\text{Hz})$ (\AA) (3)	$V_{1/2}(\text{Br}\gamma)$ (km s^{-1})		$W(\text{Br}\gamma)$ (\AA)		$F(\text{Br}\gamma)$ [$\text{Wm}^{-2} (\times 10^{-16})$]	
			1993 (4)	1996 (5)	1993 (6)	1996 (7)	1993 (8)	1996 (9)
Haro 6-37.....	23.2	26	≤ 70	...	$\leq 0.3 \pm 0.1$...	$\leq 0.1 \pm 0.03$...
Haro 6-37/c.....	19.5	191	100	...	2.9 ± 0.1	...	0.4 ± 0.04	...
AS 205.....	-2.1	155	220	...	4.0 ± 0.4	...	6.7 ± 0.7	...
AS 205/c.....	...	55	≤ 125	...	$\leq 1.4 \pm 0.3$...	$\leq 0.7 \pm 0.2$...
S CrA North.....	4.6	90	210	160	9.1 ± 0.4	7.9 ± 0.2	7.6 ± 0.4	6.5 ± 0.1
S CrA South.....	210	170	6.5 ± 0.1	5.7 ± 0.4	3.3 ± 0.1	2.9 ± 0.2
VV CrA South.....	-1.4	105	140	136	7.4 ± 0.3	12.0 ± 0.1	7.6 ± 0.3	9.2 ± 0.1
VV CrA North.....	≤ 120	145	$\leq 0.9 \pm 0.5$	2.9 ± 0.2	$\leq 0.7 \pm 0.4$	3.0 ± 0.2

NOTE.—Where only one value of V_{helio} or $W(\text{Hz})$ appears, it represents the entire system.

REFERENCES.—(1) Cohen 1974; (2) SP95; (3) This paper; (4) Glass & Penston 1975.

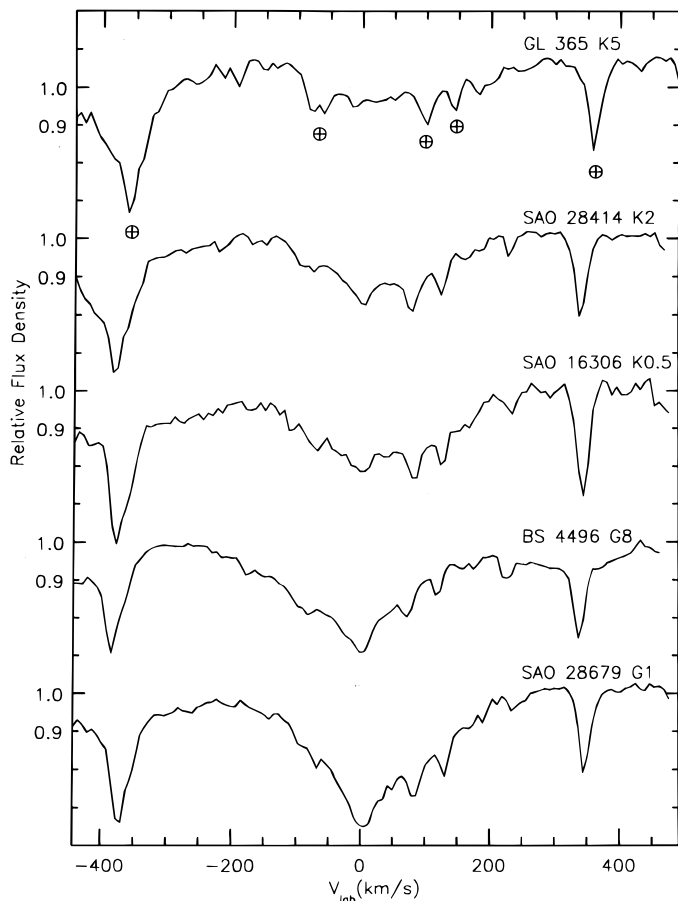


FIG. 1.— $\text{Br}\gamma$ spectra of main-sequence spectral type standards. Resolution is 20,000 for all five stars. The spectra are undivided by flux standards; prominent telluric lines are indicated by \oplus in the K5 spectrum. For purposes of comparison, the $\text{Br}\gamma$ absorption feature in each spectrum is aligned at zero velocity.

as representative of an M2–M5 V stellar spectrum; as expected, no trace of the $\text{Br}\gamma$ line is seen in the sunspot spectrum.

Flat fields were obtained using an internal quartz lamp. Subtraction of median-filtered dark fields from median-filtered flat fields eliminated dark current and dead pixels in our final flat field. Subtraction of beam-switched spectra eliminated dead pixels in the data. After flat-fielding, each pair of spectra was inspected in order to select only data with high signal-to-noise and to interpolate over spurious pixels prior to averaging all pairs. The final spectra are extracted from the average by fitting a weighted, characteristic point spread function (PSF) to each column of the array in the cross-dispersion direction. We determined the PSF by averaging several cuts across the stellar spectrum (columns on the array in the cross-dispersion direction) in a region free of spectral lines.

In 1993, we observed AS 205 and S CrA (separations $< 1''.5$) with both components on the slit. The spectra of the primary and secondary are therefore overlapping on the array. In order to separate the individual components, we used the PSF of a single star standard, observed before or after the program object at the same grating setting. We created a binary PSF by overlaying two of the single PSFs, spacing the centroids by the number of pixels corresponding to the projected separation of the binary on the slit. We then fitted the binary PSF to the data, varying the component flux and flux ratio to provide a best fit to the data in the least squares sense. In general, we binned the final, processed spectra by a factor of 2 to yield Nyquist sampling for spectra taken at 20,000 resolution. No other filtering was applied.

The circular variable filter (CVF) used to select the spectroscopic order at the time of the 1993 observations introduced a fringe intensity pattern on the array. We found that

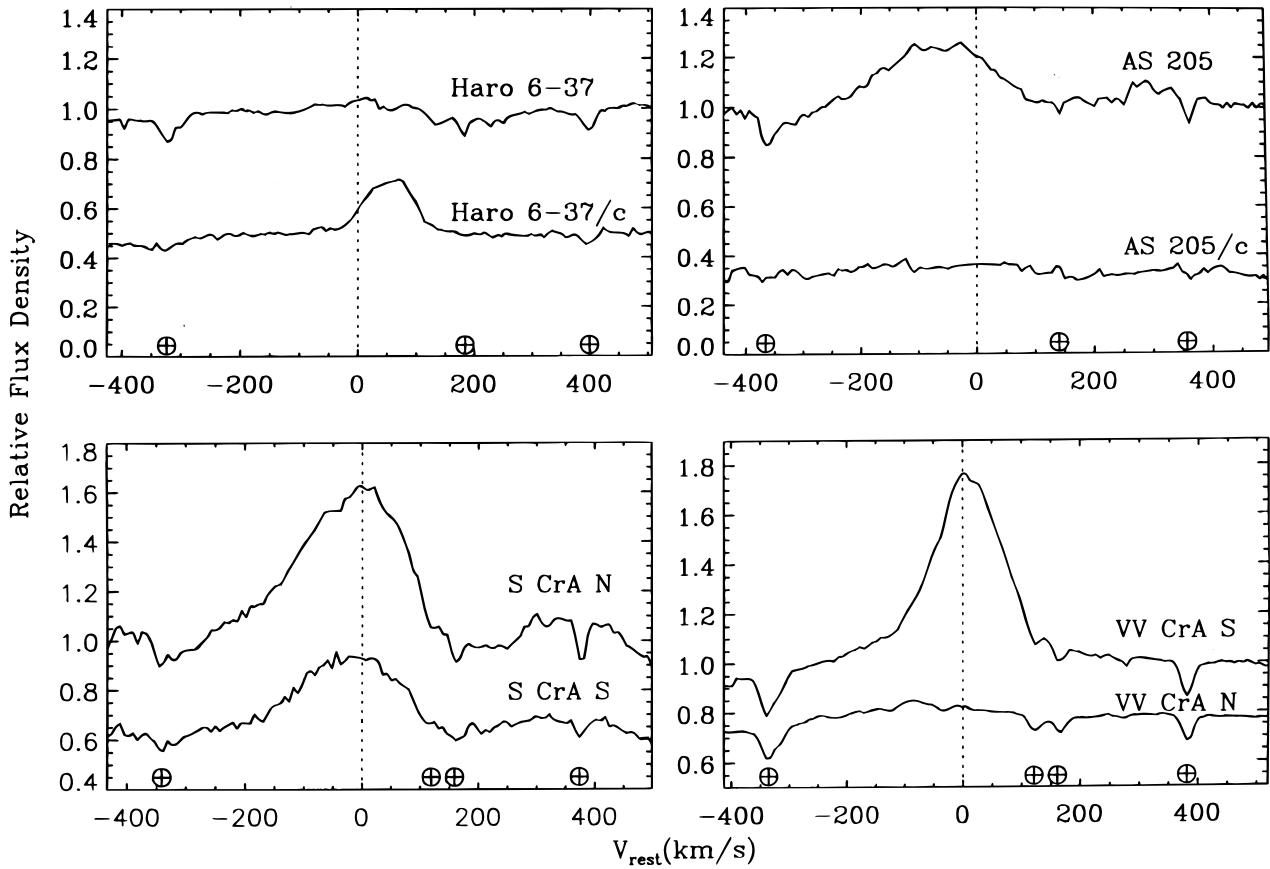


FIG. 2a

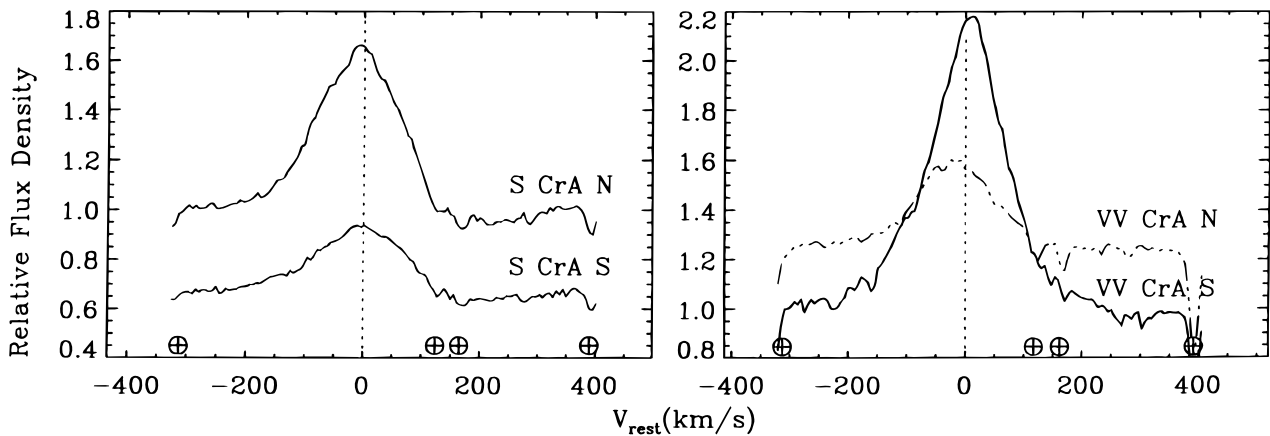


FIG. 2b

FIG. 2.— $\text{Br}\gamma$ spectra of the program objects; note the prominent emission lines in most of the components. Fringing due to internal reflections in the CVF is visible in the continuum (see text). Telluric features are indicated by \oplus . Zero velocity is the systemic rest velocity except for Haro 6-37 and its companion where zero velocity is the rest velocity of each individual star. (a) Data from 1993. For Haro 6-37 and VV CrA, $R = 20,000$, and for AS 205 and S CrA, $R = 10,000$. The $\text{Br}\gamma$ centroid of the AS 205 primary is at -60 km s^{-1} . The line centroid for Haro 6-37/c is at 50 km s^{-1} , and for S CrA and VV CrA, at 0 km s^{-1} . (b) Data from 1996. Both stars were observed at $R = 21,500$. VV CrA North is plotted with a dashed line to avoid confusion. The line centroid of both components of S CrA and of VV CrA South fall at 0 km s^{-1} systemic velocity, as in the 1993 observations. VV CrA North is blueshifted by approximately 20 km s^{-1} . The free spectral range of these observations is 730 km s^{-1} ; however, they are plotted on the same scale as the 1993 observations (free spectral range of 930 km s^{-1}).

the pattern depended on the wavelength of the observations and the illumination of the slit, varying with the position of the star along the slit and with the nature of the illumination (i.e., a point source or a continuum lamp). Division of the object spectra by the final flat field introduces additional fringing, since the fringe pattern for the continuum lamp used to obtain flat fields differs from the pattern pro-

duced by a point source. We attempted to correct for the fringing and to remove terrestrial absorption lines by dividing our spectra by early-type flux standards. Despite careful telescope guiding, however, it was not always possible to reproduce the same fringe pattern in the target and in the standard. Rather than introduce additional fringing, we did not divide our target spectra by the standard spectra; hence

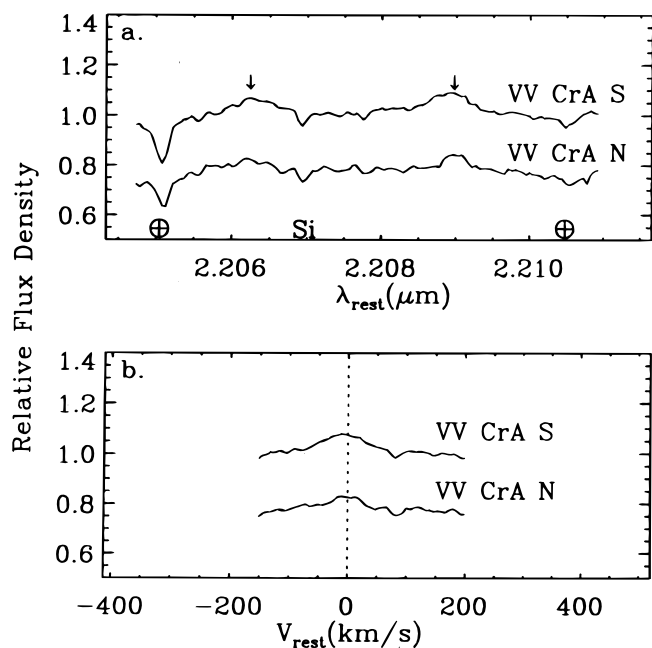


FIG. 3.—(a) The Na I 2.20 μm doublet emission of VV CrA South (S) and North (N). The spectra are plotted at the systemic rest wavelength. Telluric features are indicated with \oplus and a photospheric silicon line is marked Si. Arrows are drawn at the wavelengths of the sodium doublet. Fringing is not prominent at these wavelengths (see text). (b) Co-added Na I doublet lines are plotted on the VV CrA systemic rest velocity scale. The co-added line width of VV CrA N is about one-half that of VV CrA S.

our target and spectral type standard spectra contain uncanceled fringes and terrestrial absorption lines (see Figs. 1–3). At the wavelength of the $\text{Br}\gamma$ line, we estimate that the amplitude of the fringing was at most 8% of the continuum; at the wavelength of the Na I doublet, it was no more than 3% of the continuum. We found that, in practice, the sensitivity of our observations to spectral features was limited by these systematic effects rather than by the usual signal-to-noise considerations. We estimate conservatively that the fringing in the program object spectra results in uncertainties of $\sim 5\%$ – 10% . A CVF filter at the $\text{Br}\gamma$ wavelength was installed in CSHELL in 1994; therefore, the 1996 observations were not affected by the fringing. To calculate the line fluxes, we set the continuum to values given by available K -band photometry (see Table 4).

3. RESULTS

3.1. Spectroscopy

Figures 2 and 3 show the spectra of our program objects. The objects are listed in Table 4: Part A gives the system name (col. [1]), the HBC number (col. [2]), the spectral type (col. [3]) the component separation (col. [4]), the total K magnitude for the system (col. [5]), the log of the age calculated following SP95's procedure using the PMS evolutionary tracks of Swenson et al. (1994) (col. [6]), and the reference for the K magnitude and the age (col. [7]). Part B lists the object name (col. [1]), the heliocentric velocity of the star from Hamann (1994) (col. [2]), the $W(\text{H}\alpha)$ for both components when available, otherwise for the system as a whole (col. [3]), the velocity half-width of the $\text{Br}\gamma$ line (cols. [4]–[5]), the $W(\text{Br}\gamma)$ (cols. [6]–[7]), and the $\text{Br}\gamma$ line flux (cols. [8]–[9]). Given the fringing described in § 2.2, our ability to detect weak emission lines in Figures 2 and 3

depends on the spectral line profile. In Haro 6-37, for example, the primary may have a broad $\text{Br}\gamma$ line. Since this is difficult to distinguish from the continuum we can cite only upper limits in these cases. Therefore, the line shape and systematics described in § 2.2 dominate the errors in our estimates of $W(\text{Br}\gamma)$ and $F(\text{Br}\gamma)$.

The Haro 6-37 secondary and the AS 205 primary both show prominent $\text{Br}\gamma$ emission lines, although the spectra of the Haro 6-37 primary and the AS 205 secondary are relatively flat; in Table 4B we give upper limits only for the latter two. However, all four stars in these two systems have $W(\text{H}\alpha) > 10 \text{ \AA}$. Also, the $W(\text{Br}\gamma)$ ratios (using the detections and the upper limits) of the Haro 6-37 and AS 205 components are consistent with the $\text{H}\alpha$ ratios of the components. Thus, both stars in these systems demonstrate TT characteristics. In the 1993 and the 1996 data, S CrA shows strong $\text{Br}\gamma$ emission in both components, unambiguously identifying both of these as TTs. Note the slight asymmetry in the S CrA line profiles: there is an extended “blue wing” in both components (see Najita, Carr, & Tokunaga 1995), evident even in the 1993 data, for which no $\text{Br}\gamma$ CVF filter was available. VV CrA South displays a prominent $\text{Br}\gamma$ emission line in 1993 and in 1996. The $W(\text{Br}\gamma)$ and line flux of this component is even greater in 1996. In the 1993 data, the TT or WT nature of the northern component is not obvious, since the $\text{Br}\gamma$ region spectrum is essentially flat. However, a dramatic variation in the $\text{Br}\gamma$ line of VV CrA North is apparent in the 1996 data. The continuum level of this component is now greater than that of VV CrA South, and a prominent, slightly redshifted $\text{Br}\gamma$ emission line is clearly present, unequivocally demonstrating the TT nature of this star. In Figure 3 we present the spectrum of the 2.207 μm Na I doublet for VV CrA. We interpret the sodium emission lines as also indicative of TT activity in both components of this system, since, even for very late type stars, we expect “normal” photospheres to produce well-defined Na I absorption lines. Strong emission lines arise in energetic stellar winds and outflows as well as at the star-disk boundary layer; emission lines of a wind origin may contaminate or dominate emission-line spectra from boundary layer activity. However, since strong winds are correlated with the presence of optically thick accretion disks (Edwards et al. 1993), our conclusions are consistent with either interpretation of the emission-line origin.

3.2. Photometry

Table 3 lists K – L values for each component of the systems for which we have angularly resolved data. The system name appears in column (1), the HBC number in column (2), and the system separation in column (3). The log of the system age (col. [4]) is based on the Swenson PMS evolutionary tracks. We used ages from SP95 when available, and for FV Tau and Haro 6-10 we calculate ages as in SP95. In columns (5) and (6) we give the K – L colors for the two components, and, in column (7), the reference for the K – L s. In every case the K – L value of both components in the systems studied is greater than 0.4 mag, implying the presence of optically thick disks (Edwards et al. 1993). This includes Ck St 3, although this system has been classified by unresolved, $\text{H}\alpha$ spectroscopy as a WT (HBC). The binary DD Tau has been resolved by $\text{H}\alpha$ imaging (Bouvier, Tessier, & Cabrit 1992), as well as photometrically (Tessier, Bouvier, & Lacombe 1994). For the northern component, $W(\text{H}\alpha) = 240 \text{ \AA}$, and for the southern component,

$W(H\alpha) = 125 \text{ \AA}$. This result is consistent with the $K-L$ TT classification of both components. Herbst, Koresko, & Leinert (1995) used $R \sim 360$ grism spectroscopy to study both components in the Haro 6-10 and UY Aur systems. Haro 6-10 A and UY Aur B display prominent $\text{Br}\gamma$ emission lines.

3.3. Overview

For all of the 12 objects in our sample, we find that if the unresolved system was initially characterized as a TT, then the components, resolved, both show TT characteristics. Thus, TT activity in a previously unresolved binary is attributable to both components, although it is common that one star dominates. The dominant TT component can be either the brighter or the fainter object in continuum emission. The ages of the systems studied range from 5.0×10^4 to 2.0×10^6 yr (see Tables 3 and 4), representative of the ages in the SP95 sample, so we do not believe that this result is the effect of an age bias.

4. DISCUSSION

4.1. TT Evolution

4.1.1. The Dissipation Process

We interpret the criteria for the characterization of young stars that we have examined in this work in terms of the implications for the evolution of circumstellar accretion disks. Strong $H\alpha$ and $\text{Br}\gamma$ emission lines are one indication of the presence of relatively dense disks that feed boundary layer accretion. $K-L$ colors in excess of stellar photospheric values indicate the presence of optically thick, circumstellar material, probably in a disk structure, since the objects studied here are optically visible. In § 3 we used these criteria to show that both stars in the close binary systems studied, spanning a large range of ages, retain their innermost disks for approximately the same length of time. SP95 show that the observable stage of disk dissipation, that is, the transition from an optically thick to an optically thin disk, proceeds relatively rapidly in both singles and binaries, probably in less than 10^5 yr. Taken together, these results indicate that individual inner disks do not dissipate randomly, nor does the dissipation mechanism and time-scale vary significantly for singles and binaries. This is in contrast to the finding that the structure of outer disks in binary systems evolves more rapidly than in single systems (Osterloh & Beckwith 1994; Jensen et al. 1996; Dutrey et al. 1996). In the Taurus SFR, the binary separation distribution peaks at approximately 40 AU. Hence, it is not surprising that the outer disks are more strongly affected, since the stars literally orbit through the region that would be occupied by the unperturbed disk of a single star. For very small separation binaries ($\lesssim 10$ AU), it is likely that inner disks would be disrupted, owing to the presence of a companion. However, in the sample considered in this paper (separations of 40–360 AU), inner disks of several AU extend at most to about 1/10 of the binary separation. Our results indicate that binaries in this separation range, as well as singles, are influenced by some process sufficiently global to affect a system of two stars at one time and yet sufficiently local for the observable disk dissipation not to occur simultaneously for all stars in a subgroup, since we know that such subgroups are composed of both WT and TT systems, at least in the Taurus SFR (Gomez et al. 1993). In the following subsection we discuss a possible mechanism

to explain our results. Here we consider the process of disk dissipation by examining the NIR colors of a large sample of PMS singles and binaries in the context of our results in this current work.

Consider a flat, optically thick reprocessing disk around a $1 L_{\odot}$ star of temperature T_{\odot} . The Wien temperatures of the K , L , and N band radiation in the disk arise from regions at radii of ~ 0.06 AU, ~ 0.12 AU, and ~ 0.49 AU, respectively. Thus, the $K-L$ color provides a diagnostic of the very innermost disk, and the $K-N$ color, of the inner $\frac{1}{2}$ AU of the disk. For optically thin disks around WTs, we expect values of $K-L < 0.4$ and $K-N < 1.0$. Values of $K-L > 0.4$ and $K-N > 2.0$ are characteristic of the optically thick disks expected in TT systems (Edwards et al. 1993; SP95). Using dust grain opacities estimated by Draine & Lee (1984), and the typical radius for which an optical depth of unity is reached at 1.3 mm from Osterloh & Beckwith (1994), we apply a $p = -1.5$ power-law disk surface density distribution to calculate typical $2 \mu\text{m}$ optical depths at disk radii of 1 AU. We find values on the order of 10^5 . Therefore, all but 0.001% of the disk mass must be dissipated before we will begin to see the evidence for a transition to an optically thin disk at $2 \mu\text{m}$. This last phase, compared to the lifetime of the disk, is very brief.

In Figure 4a we plot $K-L$ versus $K-N$ colors for the 26 unresolved binary systems from the sample used for analysis in SP95; all $K-L$ data is taken from Strom et al. (1989) and Simon et al. (1995). No objects have been observed with values of $K-N$ between 1.0 and 2.0 (see Skrutskie et al. 1990; SP95). We delineate this gap in Figure 4 and also plot a dashed line at $K-L = 0.4$ for reference. According to the cutoff values for classic TT behavior described above, we define four sectors in Figure 4a: TT, WT, and the hybrid sectors H1 and H2. H2 is located below the $K-L$ cutoff for TT activity, but above the $K-N$ cutoff. For H1, the reverse is true. There are 17 binaries in the TT sector and 8 in the WT sector. CK St 3 is indicated with an asterisk (see § 3.2) in Figure 4a. That no objects are observed in H1 possibly indicates that inner disks which are optically thick at $2.2 \mu\text{m}$ yet optically thin at $10 \mu\text{m}$ are extremely rare. The binaries DI Tau (WT) and ZZ Tau (TT) lie in H2. Either disks in these systems may contain inner gaps, or these stars may represent mixed TT/WT pairs. Reddening may shift objects from H2 into the TT quadrant (Fig. 4a shows the reddening vector for the van de Hulst No. 15 extinction curve), but is otherwise not likely to affect positions of systems in Figures 4a and 4c.

To investigate whether the distribution of binaries in Figure 4a could be the result of chance, we formed model binaries by random pairing of single WTs and TTs. The single stars, and their K , L , and N band photometry, are drawn primarily from SP95. We used 52 single stars in order to form 26 boundaries. Of the 52 stars, 56% are WTs, since this fraction is required to produce a statistical average of eight pure WT pairs, as observed and plotted in Figure 4a (see above). Therefore, specific WTs appear more than once in the sample because we could identify only eight single stars in Taurus that are WTs both in terms of emission line and color criteria, with known K , L , and N magnitudes. We first randomly add, subtract, or leave out 0.1 magnitudes of noise to the K , L , and N magnitudes of the sample stars, principally to introduce variations in the duplicates. We then calculate the corresponding K , L , and N band fluxes of the 52 stars. In a single trial, the stars are

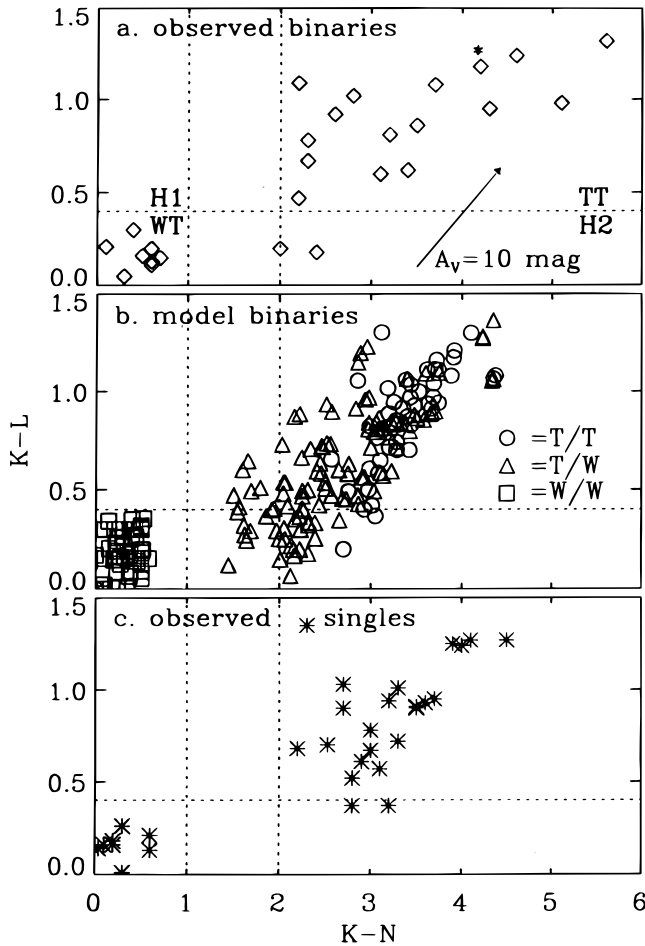


FIG. 4.—NIR colors for observed binaries, simulated binaries, and observed singles. Vertical dashed lines delineate the gap between $K-N$ of 1 and 2, and a horizontal line marks the TT cutoff at $K-L = 0.4$ (see text). (a) $K-L$ vs. $K-N$ for the sample of observed binaries from SP95. The two systems in the H2 sector, DI and ZZ Tau, are discussed in the text. CK St 3 is plotted with an asterisk. The four sectors, WT, TT, H1, and H2, and the reddening vector, are indicated. (b) $K-L$ vs. $K-N$ for 260 simulated binary systems, composed of randomly paired TT and WT singles. (c) $K-L$ vs. $K-N$ for the sample of observed single stars from SP95.

then randomly paired into 26 binaries. The fluxes of the binaries are added, and the simulated binary magnitudes and colors derived. Figure 4b shows the model system colors for 10 trials. Of the total number of simulated binaries formed in 100 random pairing trials, 31% are WT/WT pairs (as required), 19% are TT/TT pairs, and 50% are TT/WT pairs. 53% of the simulated systems are located in the TT quadrant; of the total number of systems in this quadrant, 64% of them are actually mixed TT/WT pairs. Therefore, if binary star formation were the result of random pairing, we would expect that a sample of unresolved, close binaries characterized as TTs, when resolved, would be found to consist of approximately $\frac{2}{3}$ mixed pairs. However, as we described in § 3, we do not find any mixed TT/WT pairs among the resolved TT binary systems. The fact that the single stars used to model the randomly paired binaries may have a different evolutionary history than those in real binaries is a weakness in our simulation. Also, we do not strictly pair only stars of similar ages. Nonetheless, our modeling strongly suggests that binary systems are not composed of randomly paired stars, and therefore that a common local environment plays a significant role in the

evolution of the inner disks.

In Figure 4c we plot $K-L$ and $K-N$ colors for the singles from the SP95 sample. To be located in the H2 sector, a single star must have some peculiarity in its disk structure, such as an inner hole or a gap in the disk. The position of the two stars, CX Tau and GM Aur, at the edge of the H2 sector is ambiguous, since reddening (see Fig. 4a) and/or the uncertainty in their colors (approximately the plotting symbol size) is enough to place them in the TT sector or farther inside the hybrid sector H2. The nature of the H2 sector binaries, DI Tau and ZZ Tau, is also ambiguous. If the H2 singles do correspond to objects located in the H2 sector, then they and the H2 binaries could represent objects with inner disk gaps or partially dissipated disks. If CX Tau and GM Aur are located in the TT sector, it is possible that DI Tau and ZZ Tau have NIR colors characteristic of mixed WT/TT binaries. In our plot of randomly paired model binaries (Fig. 4b), many mixed systems fall in the H2 sector. Although no resolved binary systems observed have been found to be mixed, all of the 12 systems examined in this paper, plotted as unresolved points in the $K-L$ versus $K-N$ plane, are located in the TT sector. If DI Tau and ZZ Tau are WT/TT pairs, then the location in the H2 sector of just two systems from the SP95 sample probably indicates that mixed pairs evolve very rapidly into WT/WT pairs. Note that the $W(H\alpha)$ value for both DI Tau and ZZ Tau is relatively small, 2 Å and 15 Å, respectively, while it is 20 Å and 96 Å, respectively, for CX Tau and GM Aur.

To investigate the possible dependence of the TT/WT nature of the stars in a binary on separation, we used data from Hartigan, Strom, & Strom (1994) and examined the occurrence of mixed TT/WT pairs in two ranges of binary separation. Out of eight systems with separations between 3'' and 10'', only one is a mixed system. In contrast, for the 13 systems with separations between 10'' and 50'', eight of the pairs are mixed. Possibly a significant fraction of the Hartigan et al. binaries with separations greater than 10'' are actually not physically related pairs. Alternatively, the conditions or mechanism responsible for the coupled disk dissipation in binary stars could be limited to a range of approximately 10''.

4.1.2. The Dissipation and Replenishment Mechanism

The problem posed by our observational result is the nature of the disk dissipation and replenishment. We compared accretion disk lifetimes to stellar ages for eight stars in SP95 which are older than 10^6 yr yet have retained their accretion disks as indicated by a $K-N$ color greater than 2.0. From data in Strom et al. (1989) we derived accretion rates for this sample (four binary and four single stars) based on the difference between the total luminosity and the stellar luminosity for each system, assuming that this difference represents the accretion luminosity. Combining stellar accretion rates with disk mass estimates from the 1.3 mm and 2.7 mm observations of Osterloh & Beckwith (1994) and Dutrey et al. (1996), respectively, we calculated accretion disk lifetimes. With one exception, accretion disk lifetimes are smaller than stellar ages, implying that, for the given rate of accretion, it is necessary to replenish most disks in order that their ages be consistent with those of the stars. This problem could be particularly acute in the case of binary systems, since the outer disk structure is truncated and dissipated by the orbital dynamics, if in-plane feeding of

the inner disk is completely cut off.

All 12 systems studied in this paper show a mid-IR excess and all are characterized as class II sources by Kenyon & Hartmann (1995). Specifically, the *IRAS* data (Strom et al. 1989) indicate that these systems have SEDs that show a relatively flat distributions in λF_{λ} . The theoretical results of Calvet et al. (1994) and Calvet (1995) indicate that the presence of a circumstellar or circumbinary envelope should give rise to flat spectrum sources. We therefore considered the replenishment of the disk material by out of plane flow from an optically thin, flattened envelope or shell surrounding the PMS single or binary system (Adams, Lada, & Shu 1987; Whitney & Hartmann 1992, 1993; Natta 1993; Calvet 1995). Using the Calvet et al. (1994) model for accretion from such an envelope, we find that for typical stellar masses and densities of the infalling material, rates of accretion onto disks range from 3×10^{-5} to $1 \times 10^{-7} M_{\odot} \text{ yr}^{-1}$. Stellar accretion rates are on the order of 10^{-7} to $10^{-8} M_{\odot} \text{ yr}^{-1}$. Thus, typical envelope infall appears sufficient to replenish a typical disk. Since a circumbinary envelope can supply the disks around both stars in a binary, cessation of envelope infall initiates the disk dissipation phase for both stars simultaneously. The envelope model not only provides an adequate description of the observations presented here and in SP95, but is also supported by observations of spectral energy distributions (Adams et al. 1987; Mathieu, Adams, & Latham 1991) and polarization measurements (Ménard et al. 1993).

4.2. Implications for Binary Formation Mechanisms

In the model of McDonald & Clark (1994), a coeval cluster forms by prompt initial fragmentation and then evolves dynamically into a group of single and binary star systems with approximately equal ages and equal rates of evolution. Because accretion disks increase the effective cross-sectional area of a system, they find that young stars with disks are about 3 times more likely to form binaries than diskless stars. Their model satisfactorily explains the presence of many pure TT binary systems; however, it is inconsistent with the observed lack of mixed TT/WT systems in the range of separations that we have studied, since we would expect that some mixed systems could form by the same capture scenario, although with less frequency than the pure TT systems. In addition, it is not known how the dynamical evolution described by McDonald & Clark (1994) would effect the circumstellar/circumbinary envelope model, but it is likely that the capture event would be highly disruptive. In fragmentation models (e.g., Bonnell 1994), both stars in a binary system share a common environment and evolutionary history. Therefore, fragmentation as a for-

mation mechanism for binary stars provides a more likely description of star formation in a region such as Taurus in the context of the observations presented in this paper.

5. SUMMARY

We have studied 12 spectroscopically or photometrically resolved, close (0'3–2'6) binary TT systems and find that, in every case, both component stars have demonstrated TT behavior during the history of their observation. In contrast, resolved binaries of larger separations ($> 3''$) include mixed TT/WT pairs, which increase in number with increasing average separation. Noting that the last step in the evolution from the TT to the WT phase takes place on relatively short timescales, we examine the SP95 sample of binaries and singles in terms of the $K-L$ and $K-N$ colors of the systems. We conclude that it is highly unlikely that the components in the close binaries studied evolve independently of each other. It appears that systems in which one color indicates TT activity and the other color indicates WT activity may be composed of stars with inner disk holes or gaps, or, alternatively, may represent mixed TT/WT pairs. Our ability to distinguish between these possibilities is limited by the small sample size. In general, we cannot extrapolate these results to extremely close ($< 0'3$) binaries, since very small separations correspond to the size of the accretion disk, and the effects of this proximity probably dominate disk evolution.

We propose that depletion of “circumsystem,” optically thin, residual dust envelopes terminates accretion disk feeding. This then results in a roughly coeval (within $\sim 10^5$ yr) transition in the disk optical depth, from $\tau > 1$ to $\tau < 1$, for both stars in a binary. Evidence suggesting that disk lifetimes are, in some cases, as much as 10 to 100 times smaller than stellar ages requires this disk replenishment. The SEDs of the systems considered in this work are relatively flat, consistent with the envelope models of Calvet et al. (1994 and Calvet 1995). Further spatially resolved observations of PMS binaries are necessary to determine the robustness of this interpretation of our results.

We thank the IRTF Director and TAC for observing time and acknowledge technical assistance from J. Carr, T. Greene, F. Hamann, and J. Rayner. We benefited from discussions with N. Calvet, J. Carr, and S. Strom. We are particularly grateful to T. Greene for the 1996 May observations of VV CrA, for useful discussions, and for a careful reading of an early draft. We thank J. Carr for a helpful and prompt referee's report. This work was supported in part by NSF grant AST 94-17191.

REFERENCES

- Adams, F. C., Lada, C. J., & Shu, F. H. 1987, *ApJ*, 312, 788
 Bonnell, I. A. 1994, in *ASP Conf. Proc. 65, Clouds, Cores, and Low Mass Stars*, ed. D. P. Clemens & R. Barvanis (San Francisco: ASP), 115
 Bouvier, J., & Appenzeller, I. 1991, *A&AS*, 92, 481
 Bouvier, J., Tessier, E., & Cabrit, S. 1992, *A&A*, 261, 451
 Calvet, N. 1995, private communication
 Calvet, N., Hartmann, L., Kenyon, S. J., & Whitney, B. 1994, *ApJ*, 434, 330
 Cohen, M., & Kuhl, L. V. 1979, *ApJS*, 41, 743
 Draine, B. T., & Lee, H. M. 1984, *ApJ*, 285, 89
 Dutrey, A., Guilloteau, S., Duvert, G., Prato, L., Simon, M., Schuster, K., & Ménard, F. 1996, *A&A*, 309, 493
 Edwards, S., Ray, T., & Mundt, R. 1993, in *Protostars and Planets III*, ed. E. H. Levy and J. I. Lunine (Tucson: Univ. Arizona Press), 567
 Ghez, A. M., Neugebauer, G., Gorham, P. W., Haniff, C. A., Kulkarni, S. R., Matthews, K., Koresko, C., & Beckwith, S. 1991, *AJ*, 102, 2066
 Ghez, A. M., Neugebauer, G., & Matthews, K. 1993, *AJ*, 106, 2005
 Glass, I. S., & Penston, M. V. 1975, *MNRAS*, 172, 227
 Gomez, M., Hartmann, L., Kenyon, S. J., & Hewett, R. 1993, *AJ*, 105, 1927
 Graham, J. A. 1992, *PASP*, 104, 479
 Greene, T. P., & Meyer, M. R. 1995, *ApJ*, 450, 233
 Greene, T. P., Tokunaga, A. T., Toomey, D. W., & Carr, J. S. 1993, *SPIE*, 1946, 313
 Haas, M., Leinert, Ch., & Zinnecker, H. 1990, *A&A*, 230, L1
 Hamann, F. 1994, *ApJS*, 93, 485
 Hartigan, P., Strom, K. M., & Strom, S. E. 1994, *ApJ*, 427, 961
 Herbig, G. H., & Bell, K. R. 1988, *Lick Observatory Bull.* 1111 (HBC)
 Herbst, T. M., Koresko, C. D., & Leinert, Ch. 1995, *ApJ*, L93
 Jensen, E. L. N., Mathieu, R. D., & Fuller, G. A. 1996, *ApJ*, 458, 312
 Keenan, P., & McNeil, I. 1989, *ApJS*, 71, 245
 Kenyon, S. J., & Hartmann, L. 1995, *ApJS*, 101, 117

- Kleinmann, S. G., & Hall, D. N. B. 1986, *ApJS*, 62, 501
Leinert, Ch., & Haas, M. 1989, *ApJ*, 342, L39
Leinert, Ch., Zinnecker, H., Weitzel, N., Lenzen, R., Haas, M., Christou, J., Ridgway, S., & Jameson, R. 1993, *A&A*, 278, 129
Livingston, W., & Wallace, L. 1991, NSO Tech. Rep. 91-001 (Tucson: NSO)
Mathieu, R. D., Adams, F. C., & Latham, D. W. 1991, *AJ*, 101, 2184
McDonald, J. M., & Clark, C. J. 1994, in *ASP Conf. Proc.* 65, *Clouds, Cores, and Low Mass Stars*, ed. D. P. Clemens & R. Barvanis (San Francisco: ASP), 370
Ménard, F., Monin, J.-L., Angelucci, F., & Rouan, D. 1993, *ApJ*, 414, L117
Najita, J., Carr, J. S., & Tokunaga, A. T. 1996, *ApJ*, 456, 292
Natta, A. 1993, *ApJ*, 412, 761
Osterloh, M., & Beckwith, S. V. W. 1995, *ApJ*, 439, 288
Persson, S. E., Aaronson, M., & Frogel, J. A. 1977, *AJ*, 82, 729
Shu, F. H., Adams, F. C., & Lizano, S. 1987, *ARA&A*, 25, 23
Simon, M., et al. 1995, *ApJ*, 443, 625
Simon, M., & Prato, L. 1995, *ApJ*, 450, 824 (SP95)
Skrutskie, M. F., Dutkevitch, D., Strom, S. E., Edwards, S., Strom, K. M., & Shure, M. A. 1990, *AJ*, 99, 1187
Strom, K. M., Strom, S. E., Edwards, S., Cabrit, S., & Skrutskie, M. F. 1989, *AJ*, 97, 1451
Swenson, F. J., Faulkner, J., Rogers, F. J., & Iglesias, C. A. 1994, *ApJ*, 425, 286
Tessier, E., Bouvier, J., & Lacombe, F. 1994, *A&A*, 283, 827
Tokunaga, A. T., Toomey, D. W., Carr, J. S., Hall, D. N. B., & Epps, H. W. 1990, *SPIE*, 1235, 131
Wallace, L., & Livingston, W. 1992, NSO Tech. Rep. 92-001 (Tucson: NSO)
Whitney, B. A., & Hartmann, L. 1992, *ApJ*, 395, 529
———. 1993, *ApJ*, 402, 605